Structure

Article

Identification of an atypical interaction site in the BTB domain of the MYC-interacting zinc-finger protein 1

Graphical abstract

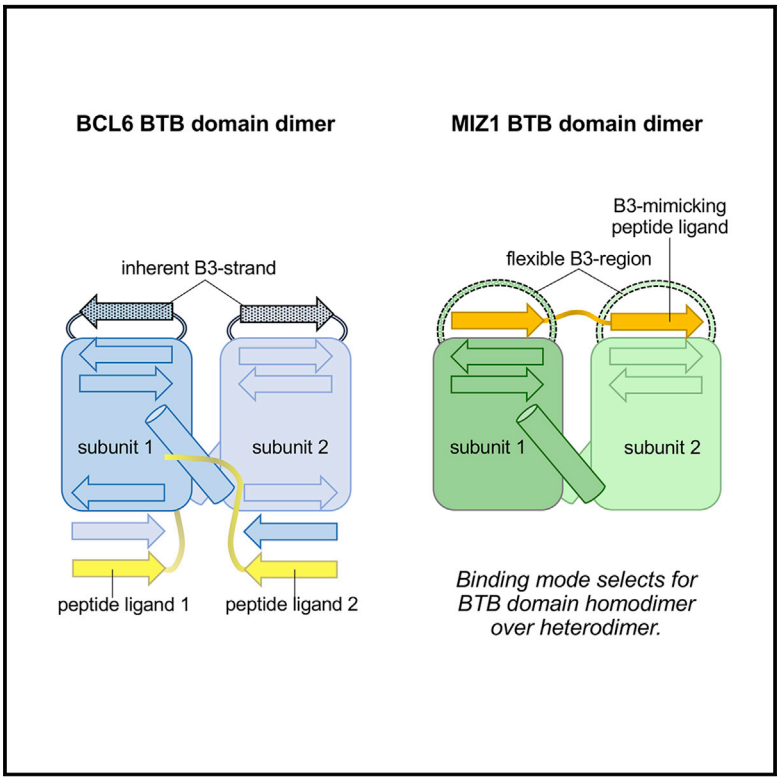

Highlights

- The BTB domain of MIZ1 harbors an atypical peptide binding site.
- This binding site requires flexibility in a core element of the BTB fold.
- Peptide binding selects for homodimers over heterodimers of the MIZ1 BTB domain.

Authors

Barbara Orth, Bodo Sander, Andreas Möglich, Kay Diederichs, Martin Eilers, Sonja Lorenz

Correspondence

sonja.lorenz@mpibpc.mpg.de

In brief

Orth et al. identify an atypical peptide binding site in the BTB domain of the transcription factor MIZ1, which requires the BTB domain to be homodimeric. The binding site highlights conformational flexibility in the core BTB fold and may hold opportunities for future therapeutic interventions with MIZ1-mediated signaling.

Orth et al., 2021, Structure *29*, 1–11
November 4, 2021
https://doi.org/10.1016/j.str.2021.06.005

CellPress

Please cite this article in press as: Orth et al., Identification of an atypical interaction site in the BTB domain of the MYC-interacting zinc-finger protein 1, Structure (2021), https://doi.org/10.1016/j.str.2021.06.005

Structure

CellPress

Article

Identification of an atypical interaction site in the BTB domain of the MYC-interacting zinc-finger protein 1

Barbara Orth,[1,2] Bodo Sander,[1] Andreas Möglich,[3] Kay Diederichs,[4] Martin Eilers,[5] and Sonja Lorenz[2,6,*]
[1]Rudolf Virchow Center for Integrative and Translational Bioimaging, University of Würzburg, 97080 Würzburg, Germany
[2]Max Planck Institute for Biophysical Chemistry, 37077 Göttingen, Germany
[3]Lehrstuhl für Biochemie, University of Bayreuth, 95447 Bayreuth, Germany
[4]Department of Biology, University of Konstanz, 78457 Konstanz, Germany
[5]Lehrstuhl für Biochemie, Biocenter, University of Würzburg, 97074 Würzburg, Germany
[6]Lead contact
*Correspondence: sonja.lorenz@mpibpc.mpg.de
https://doi.org/10.1016/j.str.2021.06.005

SUMMARY

The repurposing of structurally conserved protein domains in different functional contexts is thought to be a driving force in the evolution of complex protein interaction networks. The BTB/POZ domain is such a versatile binding module that occurs over 200 times in the human proteome with diverse protein-specific adaptations. In BTB-zinc-finger transcription factors, the BTB domain drives homo- and heterodimerization as well as interactions with non-BTB-domain-containing proteins. Which mechanisms encode specificity in these interactions at a structural level is incompletely understood. Here, we uncover an atypical peptide-binding site in the BTB domain of the MYC-interacting zinc-finger protein 1 (MIZ1) that arises from local flexibility of the core BTB fold and may provide a target site for MIZ1-directed therapeutic approaches. Intriguingly, the identified binding mode requires the BTB domain to be in a homodimeric state, thus holding opportunities for functional discrimination between homo- and heterodimers of MIZ1 in the cell.

INTRODUCTION

The evolution of complex biological functions was suggested to be driven by the reiterated use of a rather small set of protein interaction domains that may allow for a rapid expansion of protein connectivities at low genomic expense (Pawson and Nash, 2003). This implies that protein interaction domains, although structurally conserved, accommodate flexibility to refine, diversify, or change their binding properties. A growing body of data illustrates the astounding range of structural mechanisms by which this concept manifests itself, endowing individual domains with context-dependent functions. The BTB (Bric-à-brac, Tramtrack, and Broad complex) fold, also known as POZ (POx virus and Zinc finger) domain, is such an architecturally conserved yet versatile binding module that recurs in over 200 functionally diverse human proteins involved in transcriptional regulation, chromatin remodeling, cytoskeletal organization, ion channel gating, and ubiquitination (Chaharbakhshi and Jemc, 2016; Letunic and Bork, 2017). Built around a mixed α/β-core, BTB domains contain varied peripheral structural elements that control their oligomerization or association with other proteins (Aravind and Koonin, 1999; Stogios et al., 2005). For example, an N-terminal extension to the BTB core mediates homo- or heterodimerization in the BTB-kelch and MATH-BTB protein families, and the BTB-zinc-finger (BTB-ZF) class of transcription factors. BTB-domain-dependent higher-order self-association of BTB-ZF proteins was also reported and has important ramifications for their interactions with multivalent macromolecular partners, such as DNA (Katsani et al., 1999). Moreover, the transcriptional functions of BTB-ZF proteins require their BTB domain to recruit other, non-BTB-domain-containing factors, aside from mediating oligomerization.

How this may be accomplished was visualized at a structural level for the BTB-ZF-type, proto-oncogenic transcriptional repressor BCL6, whose expression is frequently deregulated in B cell lymphomas (Ye et al., 1993): the homodimeric BTB domain of BCL6 engages co-repressor proteins along a non-conserved, peptide-binding surface of each subunit, known as the "lateral groove" (Ahmad et al., 2003; Ghetu et al., 2008). Consistently, a rationally designed peptide, which blocks the lateral groove, inhibits BCL6 function in BCL6-positive lymphoma cells, triggering cell-cycle arrest and apoptosis (Polo et al., 2004). Based on this concept, various synthetic inhibitors of BCL6-co-repressor interactions have been developed, all of which target the lateral groove (Cardenas et al., 2016; Cerchietti et al., 2009, 2010; Cheng et al., 2018; Evans et al., 2014; Ghetu et al., 2008; Kamada et al., 2017; Kerres et al., 2017; McCoull et al., 2017; Sakamoto et al., 2017; Silva et al., 2007; Yasui et al., 2017). Certain lateral groove-binding compounds induce the ubiquitin-dependent proteasomal degradation of BCL6 in the cell (Bellenie et al., 2020; Kerres et al., 2017; Słabicki et al., 2020) while others have been utilized as building blocks for proteolysis-targeting chimeras (PROTACs) (McCoull et al., 2018). Together, these studies

Please cite this article in press as: Orth et al., Identification of an atypical interaction site in the BTB domain of the MYC-interacting zinc-finger protein 1, Structure (2021), https://doi.org/10.1016/j.str.2021.06.005

highlight the remarkable susceptibility of the BTB fold to small-molecule-mediated manipulations and the intriguing potential of harnessing this susceptibility for the therapeutic targeting of transcription factors. To this end, however, it is crucial to understand the determinants of specificity in macromolecular interactions of BTB domains beyond BCL6. For example, it is unclear whether the BTB domains of BTB-ZF proteins generally utilize the lateral groove for ligand recognition. Given the high variability of BTB domains at the primary sequence level and the associated poor conservation of their surfaces, it is possible that yet uncharacterized binding sites reside within this versatile fold.

Here, we explore the structural underpinnings of specialization in the BTB domain of the MYC-interacting zinc-finger protein 1 (MIZ1), a BTB-ZF-type transcription factor with critical roles in early development and multiple stages of tumorigenesis (Wiese et al., 2013). The transcriptional functions and chromatin association of MIZ1 require its BTB domain; as a consequence, deletion of this domain has deleterious consequences, such as cell-cycle arrest and apoptosis during early T and B cell development and cerebellar neurodegeneration due to deficient membrane trafficking (Kosan et al., 2010; Ross et al., 2019; Wolf et al., 2013). In line with its pivotal functions, the BTB domain drives numerous interactions of MIZ1, including the formation of homodimers and heterodimers with other BTB-containing proteins, such as BCL6, NAC1, ZBTB4, ZBTB36, and ZBTB49 (Jeon et al., 2014; Lee et al., 2012; Phan et al., 2005; Stead and Wright, 2014a; Weber et al., 2008). While heterodimerization was shown to reduce the MIZ-dependent transcription of *CDKN1A*, it remains to be elucidated how the alternative dimerization modes of MIZ1 are regulated and affect the reorganization of chromatin-associated complexes at a structural level. Moreover, it has not been studied structurally how the BTB domain of MIZ1 recognizes additional protein interactors that lack BTB domains, such as the host-cell factor 1 (HCF-1) (Piluso et al., 2002) or the HECT-type ubiquitin ligase HUWE1 (Adhikary et al., 2005).

We identified a HUWE1-derived peptide that specifically interacts with the BTB domain of MIZ1 in its homodimeric, but not heterodimeric or monomeric forms. The underlying binding mode requires specific structural features of the BTB domain of MIZ1 that may be amenable to therapeutic targeting. More broadly, our findings illustrate an additional facet of the structural versatility of the BTB fold that may allow for functional discrimination between homo- and heterodimers of MIZ1 in the cell. This adds to the structurally distinct concept of dimerization quality control, which explains the selective destabilization of BTB heterodimers by the RING-type ligase SCF-FBXL17 (Mena et al., 2018, 2020).

RESULTS

The BTB domain of MIZ1 interacts with a HUWE1-derived peptide in an atypical mode

When comparing the catalytic activities of truncated, C-terminal constructs of HUWE1 toward the physiological substrate MIZ1, we noticed that a region known as the activation segment (AS; residues 3,843–3,896) enhances ubiquitin chain elongation on MIZ1 compared with the isolated catalytic HECT domain (HECT; residues 3,993–4,374) (Figures 1A–1C). A stimulatory effect of the AS in the context of C-terminal fragments of HUWE1 compared with shorter, dimeric constructs (HUWE1^{D}, HUWE1^{Dmin}) had previously been observed and was rationalized by the ability of this segment to counteract the formation of an autoinhibited ligase dimer through intramolecular interactions with the dimerization region (Sander et al., 2017). The isolated HECT domain, however, is monomeric per se and was expected to have substrate ubiquitination activity comparable with that of a construct that includes the AS (HUWE1^{AS}; residues 3,843–4,374). To explain the activation segment-induced stimulation of MIZ1 ubiquitination, we hypothesized that the segment may be able to recruit MIZ1 to the HECT domain within the C-terminally truncated constructs studied here. In line with this idea, size-exclusion chromatography (SEC) analyses revealed complex formation between the AS and the BTB domain of MIZ1 (MIZ1^{BTB}, residues 1–115) (Figures 1D and 1E). This domain was previously shown to drive the interaction of MIZ1 with HUWE1 (Adhikary et al., 2005). We also observed a weak interaction between HUWE1^{AS}, but not HUWE1^{D}, with MIZ1^{BTB} by SEC (Figures S1A–S1D). This supports the notion that the AS can recruit MIZ1 within C-terminal fragments of HUWE1 while this interaction competes with the alternative, intramolecular association of the AS with the dimerization region. Note that the present study focuses on MIZ1 ubiquitination (Figures 1B and 1C) rather than the autoubiquitination activities of the truncated HUWE1 constructs that were discussed previously (Sander et al., 2017).

We hypothesized that the AS contains discrete sites to mediate the recruitment of MIZ1^{BTB} and intramolecular interactions within the HUWE1^{AS} construct. Guided by secondary structure predictions, we analyzed the binding properties of the N-terminal (AS^{N}; residues 3,843–3,869) and C-terminal (AS^{C}; residues 3,870–3,890) portions of the activation segment individually. SEC and fluorescence polarization (FP) experiments demonstrated that the BTB domain of MIZ1 exclusively recognizes AS^{C} (Figures 2A–2C). The corresponding dissociation constant, K_D, is in the low-micromolar range (10.0 ± 0.9 μM); no K_D value could be derived for AS^{N} (Figure 2C and Table 1). In contrast, AS^{N} provides the predominant binding site for the dimerization region (residues 3,951–3,993) within the C-terminally truncated HUWE1 fragments analyzed here (see Figure 1A). We determined K_D values of 4.9 ± 0.8 μM and 322 ± 46 μM for the interactions of AS^{N} and AS^{C} with HUWE1^{Dmin} (residues 3,951–4,374; the minimal dimerizing C-terminal fragment of HUWE1), respectively (Figure 2D).

Conformational flexibility of the B3 region enables atypical peptide recognition by the BTB domain of MIZ1

To elucidate how the BTB domain of MIZ1 recognizes the AS^{C} peptide, we determined a crystal structure of the complex at 2.25-Å resolution (Table 2; for details see STAR methods). The structure shows the dimeric BTB domain bound to a single peptide (Figure 3A). The BTB-domain dimer has a characteristic butterfly-like architecture, in which each "wing" is made up of an α-helical core flanked by β strands at the upper (B1 and B2) and lower (β5) end. The peptide ligand orthogonally traverses the subunit interface, forming a β strand on either side that complements the respective upper B1-B2 sheet. Therefore, the ligand-induced β-sheet extension follows a parallel mode in one subunit and an antiparallel mode in the other, with distinct intermolecular contacts formed in each case (Figure 3B). The structural elements of the BTB domain that make up the bipartite binding site also adopt distinct orientations in the two subunits

Please cite this article in press as: Orth et al., Identification of an atypical interaction site in the BTB domain of the MYC-interacting zinc-finger protein 1, Structure (2021), https://doi.org/10.1016/j.str.2021.06.005

CellPress

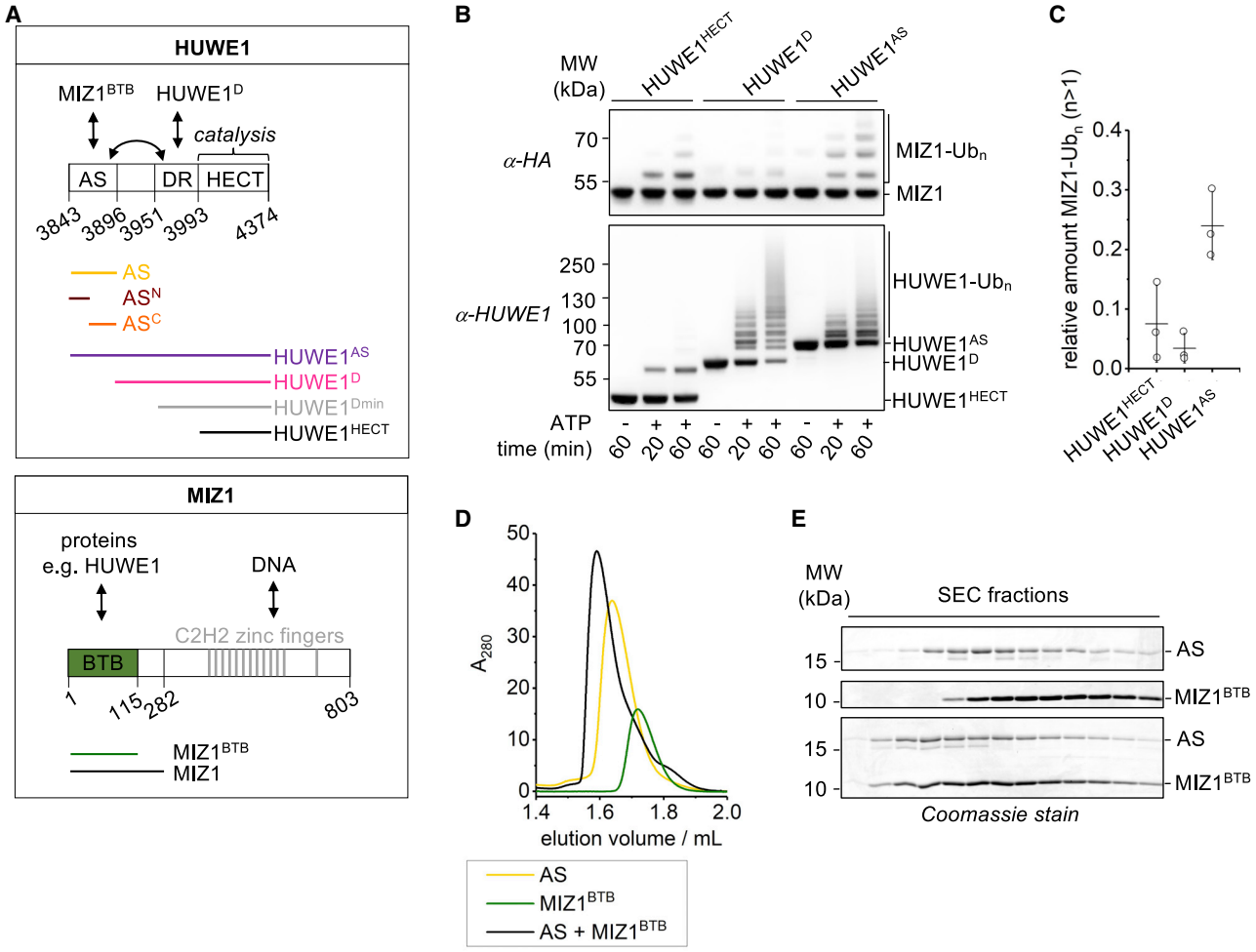

Figure 1. The BTB domain of MIZ1 interacts with a hydrophobic segment found in the C-terminal region of HUWE1

(A) Architecture of C-terminal fragments of HUWE1 (top), indicating the boundaries of the motifs and protein constructs studied here. AS, activation segment; DR, dimerization region; HECT, catalytic HECT domain. AS^N and AS^C denote the N- and C-terminal portions of AS, respectively. $HUWE1^{AS}$ and $HUWE^{HECT}$ are monomeric; $HUWE1^D$ and $HUWE1^{Dmin}$ dimerize (Sander et al., 2017). The activation segment interacts intramolecularly with the dimerization region in the context of $HUWE1^{AS}$. Lower panel: domain architecture of MIZ1, featuring the N-terminal BTB domain, which mediates protein-protein interactions, and 13 zinc fingers in the C-terminal region, which mediate DNA binding. In both panels, double arrows symbolize interactions.

(B) Representative assay comparing the ubiquitination activities of the indicated HUWE1 fragments toward HA-tagged MIZ^{1-282}. The reactions were monitored for 20 and 60 min, respectively, and visualized by SDS-PAGE and anti-HA (substrate ubiquitination; top panel) and anti-HUWE1 western blotting (E3-autoubiquitination; bottom panel), respectively. Note that the constructs have different autoubiquitination propensities (ubiquitinated HUWE1 constructs collectively labeled with "HUWE1-Ub_n"), which were studied previously (Sander et al., 2017). The anti-HUWE1 blot was only used for the quantification of the HUWE1 input.

(C) Quantification of the amount of polyubiquitinated MIZ1 after 60 min, based on three independent assays as shown in (B), normalized to the input amount of HUWE1 (minus ATP lanes). Quantification was done based on three independent replicates using the Image Studio Lite Software (Li-COR; Lincoln, NE, USA; RRID: SCR_013715). The mean and standard deviations were plotted.

(D) SEC analysis of the interaction between $MIZ1^{BTB}$ and AS (HUWE1 residues 3,843–3,890 with an N-terminal lipoyl domain tag).

(E) Protein-containing elution fractions from the SEC runs shown in (D), analyzed by SDS-PAGE and Coomassie staining. The three gels are associated with the SEC analysis of AS only, $MIZ1^{BTB}$ only, and the AS-$MIZ1^{BTB}$ mixture (from top to bottom). Equivalent elution fractions of the three runs were aligned with each other.

due to different crystal contacts, as discussed below. Nevertheless, the two binding sites of the $MIZ1^{BTB}$ dimer comprise overlapping networks of hydrophobic residues, including Phe28, Leu52, Phe53, Val60, Leu62, and Ile64.

The binding mode observed for $MIZ1^{BTB}$ is distinct from other known BTB domain-peptide interactions, as illustrated by the complexes of the transcriptional repressor BCL6 with peptides derived from its co-repressors BCOR and SMRT, respectively (Figure 3C) (Ahmad et al., 2003; Ghetu et al., 2008). In those cases, the BTB-domain dimer associates with two peptides symmetrically along the lateral grooves of the subunits, with the N-terminal region of each peptide extending a mixed β sheet (β1′–β5, β1–β5′) at the lower end of each subunit. The peptide-mediated β-sheet extension in BCL6 thus occurs at the opposite face of the BTB domain compared with MIZ1. Notably, in $BCL6^{BTB}$, the upper B1-B2 sheet is complemented

Please cite this article in press as: Orth et al., Identification of an atypical interaction site in the BTB domain of the MYC-interacting zinc-finger protein 1, Structure (2021), https://doi.org/10.1016/j.str.2021.06.005

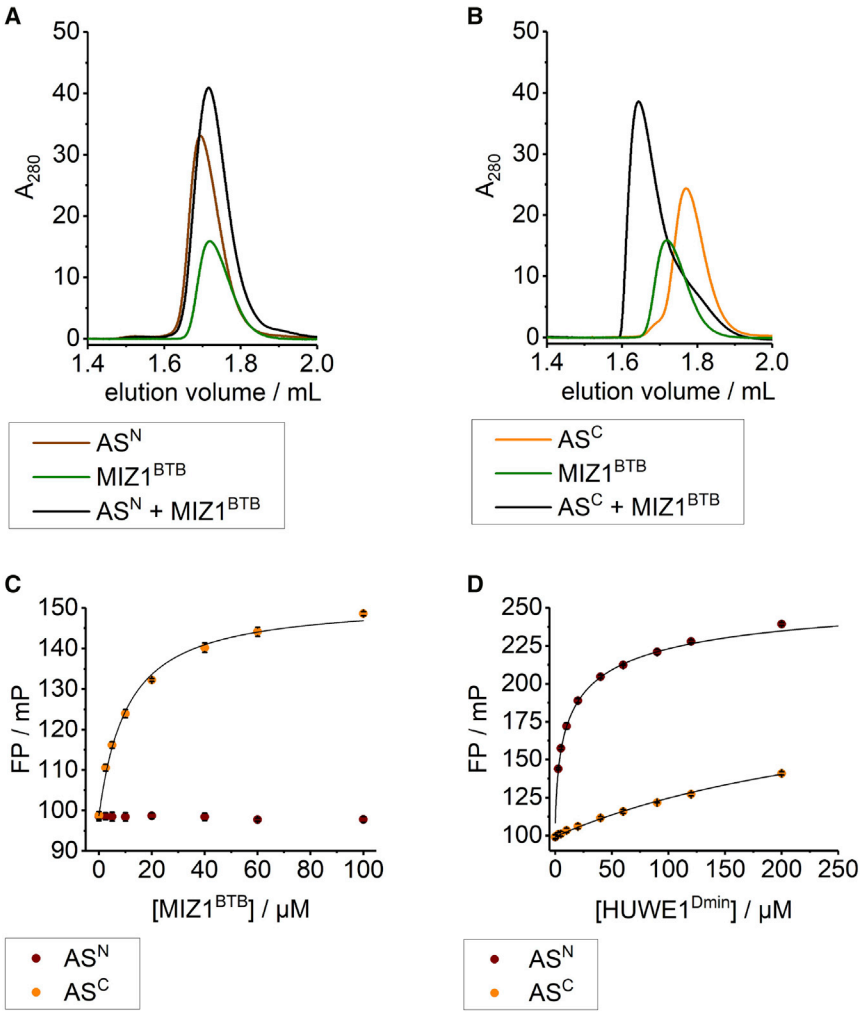

Figure 2. The C-terminal portion of the activation segment of HUWE1 mediates MIZ1 binding

(A) SEC experiments testing an interaction between $MIZ1^{BTB}$ and AS^N (HUWE1 residues 3,843–3,869 with an N-terminal lipoyl domain tag).

(B) SEC experiments testing an interaction between $MIZ1^{BTB}$ and AS^C (HUWE1 residues 3,870–3,890 with an N-terminal lipoyl domain tag). For MIZ^{BTB} the same elution profile as in (A) is shown.

(C) FP analysis of the interaction between $MIZ1^{BTB}$ and the 5-FAM-labeled AS^N and AS^C peptides, respectively. The data points represent the mean and SD of three independent experiments. The data for AS^C were fitted to a single-site binding model; for the K_D value, see Table 1. The data for AS^N could not be fitted.

(D) FP analysis of the intramolecular interaction between $HUWE1^{Dmin}$ (residues 3,951–4,374; minimal dimerizing C-terminal HUWE1 fragment) and the 5-FAM-labeled AS^N and AS^C peptides, respectively. The mean and SD of three independent experiments were fitted to a competition model that accounts for protein-ligand binding and protein dimerization; the corresponding K_D values are 4.9 ± 0.8 µM and 322 ± 46 µM for AS^N and AS^C, respectively.

intramolecularly by a third β strand (B3) that constitutes a core element of the BTB fold. The corresponding region ("B3 region") in $MIZ1^{BTB}$, however, appears flexible, allowing for an equivalent B3 strand to be provided by the AS^C peptide. The peptide ligand therefore mimics a structural element of the canonical BTB fold.

To further illuminate the atypical nature of $MIZ1^{BTB}$, we determined a crystal structure of the apo form (2.1-Å resolution; Table 2). As seen for the peptide-bound complex, the B3 region does not adopt a β strand in this structure but forms a loop that is swung outward and leaves the peptide-binding site exposed (Figure 3D). Atypical arrangements of the B3 region compared with canonical B3-containing BTB domains were also observed in previous, unrelated crystal forms of *apo* $MIZ1^{BTB}$ (PDB: 2Q81 and PDB: 3M52 [Stead et al., 2007; Stogios et al., 2010]). Only one out of six BTB subunits extracted from these structures contains an inherent B3 strand (Figure S2); in this case, however, the strand is part of an intermolecular β sheet within a crystallographic tetramer, which we and others did not detect in solution (Stead et al., 2007; Stogios et al., 2010). In sum, these analyses corroborate the notion that the lack of a pre-formed B3 strand and associated plasticity of the B3-region in $MIZ1^{BTB}$ do not result from crystal packing but represent a specific property of this BTB domain (Stogios et al., 2010).

Structure-guided mutagenesis supports the atypical peptide-recognition mode of the BTB domain of MIZ1 in solution

In line with the crystal structures we determined and previous studies (Stogios et al., 2010), SEC-coupled multi-angle light scattering (MALS) analyses showed that $MIZ1^{BTB}$ is dimeric in solution (Figure S3A). SEC-MALS and isothermal titration calorimetry (ITC) analyses of the interaction between the $MIZ1^{BTB}$ dimer and AS^C corroborate a 2:1 stoichiometry, as seen crystallographically (Figures S3A and S3B). In contrast, other BTB-peptide interactions display a 1:1 stoichiometry (Ahmad et al., 2003; Ghetu et al., 2008; Sakamoto et al., 2017).

To test whether the atypical peptide-binding mode of $MIZ1^{BTB}$ seen in the crystal structure also occurs in solution, we analyzed the effects of structure-guided mutations at key sites in the hydrophobic interface on AS^C binding. These mutations included F28A, L52A, F53A, V60P, H61A, L62A, and I64A in $MIZ1^{BTB}$ and L3877A, L3879A, F3886A, F3887A, and L3877A/F3887A in AS^C, respectively (Figures 4A and 4B). In line with the crystal structure, residues that contribute to the ligand-binding sites in both BTB subunits, such as Phe28, Leu62, and Ile64, are required for peptide binding in the low-micromolar K_D range (Figure 4A; Table 1). Furthermore, the V60P substitution in the B3 region was found to markedly weaken the interaction. This mutation was designed to interfere with the formation of a β-strand-like element, observed alongside the peptide-derived β strand in subunit 1 of the crystal (Figures 3B [left panel] and S4A). The peptide-bound B3 region of subunit 2 may adopt a similar, β-strand-like conformation in

Please cite this article in press as: Orth et al., Identification of an atypical interaction site in the BTB domain of the MYC-interacting zinc-finger protein 1, Structure (2021), https://doi.org/10.1016/j.str.2021.06.005

CellPress

Table 1. Dissociation constants

Protein	Peptide ligand	K_D (μM)	Method
MIZ1^{BTB} variant			
WT	AS^C	10.0 ± 0.9	FP
WT	AS^C	3.1 ± 0.7	ITC
F28A	AS^C	ND	FP
L52A	AS^C	9 ± 1	FP
F53A	AS^C	15.8 ± 1.5	FP
V60P	AS^C	60 ± 2	FP
H61A	AS^C	16.9 ± 1..2	FP
L62A	AS^C	88.8 ± 8.1	FP
I64A	AS^C	ND	FP
WT	AS^C L3877A	ND	FP
WT	AS^C L3879A	33.2 ± 1.6	FP
WT	AS^C F3886A	ND	FP
WT	AS^C F3887A	ND	FP
WT	AS^C L3877A/ F3887A	ND	FP
WT	AS^N	ND	FP
MIZ1^{BTB} variant (without cloning overhang)			
WT (residues 1–115)	AS^C	10 ± 1	FP
V10D/L14D/Q17D/V41K (monomer)	AS^C	ND	
MIZ1-BCL6 heterodimer	AS^C	121 ± 22	FP
MIZ1-NAC1 heterodimer	AS^C	187 ± 20	FP

ND, not determined.

Table 2. X-ray crystallographic data collection and refinement statistics

	MIZ1^{BTB}	MIZ1^{BTB}–AS^C complex
PDB	7AZW	7AZX
Data collection		
Wavelength (Å)	1.0332	0.968
Resolution (Å)	48.05-2.10 (2.16-2.10)	37.72-2.25 (2.40-2.25)
Space group	I121	P3121
Unit cell parameters		
a, *b*, *c* (Å)	48.79, 34.52, 172.56	69.11, 69.11, 97.15
α, β, γ (°)	90, 96.18, 90	90, 90, 120
Total reflections	76,616 (6,616)	308,484 (12,141)
Unique reflections	17,046 (1,417)	9,023 (450)
R_{pim}	0.069 (0.561)	0.066 (0.684)
Completeness (%)	99.8 (99.9)	68.0 (18.8)
$I/\sigma(I)$	7.4 (1.2)	13.8 (1.5)
Multiplicity	4.5 (4.7)	34.2 (27.0)
Wilson *B* factor	31.7	60.5
$CC_{1/2}$	0.996 (0.789)	0.999 (0.622)
Refinement		
Resolution (Å)	35.17–2.10 (2.175–2.10)	34.56–2.248 (2.328–2.248)
Reflections used	16,959 (1,684)	9,011 (230)
R_{work}/R_{free}	23.92/28.31	22.80/27.97
No. of atoms		
Proteins	1,805	1,941
Ligands	6	–
Water	25	16
Average *B* factors (Å^2)		
Proteins	46.0	52.4
Ligands	44.4	–
Water	35.7	35.5
RMSD from ideality		
bond lengths (Å)	0.002	0.003
bond angles (°)	0.47	0.48
Ramachandran statistics		
favored (%)	96.94	97.96
disallowed (%)	0.00	0.00
MolProbity clash score	4.43	4.41

Values in parentheses correspond to the highest-resolution shell. RMSD, root-mean-square deviation.

solution; in the crystal, however, this region is tilted outward due to lattice contacts (Figures 3B [right panel] and S4A). Other residues that contribute to the environment of the bound peptide only in one subunit (Phe53) or more peripherally (Leu52, His61) had minor or no effects on the interaction detected in solution. Notably, none of the mutated MIZ1^{BTB} variants showed defects in dimerization compared with the wild type (WT), as confirmed by SEC (Figure S4B). In additional control experiments, we interrogated the possible influence of a six-residue, cloning-induced overhang of our MIZ1^{BTB} construct on the interaction with AS^C. In the crystal structures, this overhang mimics an N-terminal β1 strand, which is not part of the BTB domain of MIZ1 but is found in other BTB domains, where it engages in a domain-swapped β1-β5′ sheet (Figure S4A). Encouragingly, MIZ1^{BTB} constructs with and without this cloning overhang did not display any differences in their oligomerization state or binding to AS^C (Figures S4B and S4C; Table 1). This corroborates the conclusion that the BTB domain of MIZ1 engages the AS^C peptide in an atypical manner that is independent of the lower β1-β5 sheet involved in peptide-binding to BCL6 (Ahmad et al., 2003; Ghetu et al., 2008).

We next interrogated the effects of mutations in AS^C on the interaction with MIZ1^{BTB}. FP-based analyses using fluorophore-labeled AS^C-peptide variants revealed drastic binding defects of the L3877A, F3886A, F3887A, and L3877A/F3887A variants compared with the WT, and a more moderate defect of L3879A (Figure 4B and Table 1). Except for F3886A, these effects are consistent with the interaction mode seen in the crystal (Figure 3B). We speculate that the significance of Phe3886 reflects the possibility that the AS^C peptide binds to MIZ1^{BTB} in more than one register or mode in solution. Different binding modes may be enabled by the extended stretch of hydrophobic residues in both β-strand portions of the peptide and the five-residue spacer connecting them (Figure 3B). Alternative explanations for the requirement of Phe3886 in peptide binding,

Please cite this article in press as: Orth et al., Identification of an atypical interaction site in the BTB domain of the MYC-interacting zinc-finger protein 1, Structure (2021), https://doi.org/10.1016/j.str.2021.06.005

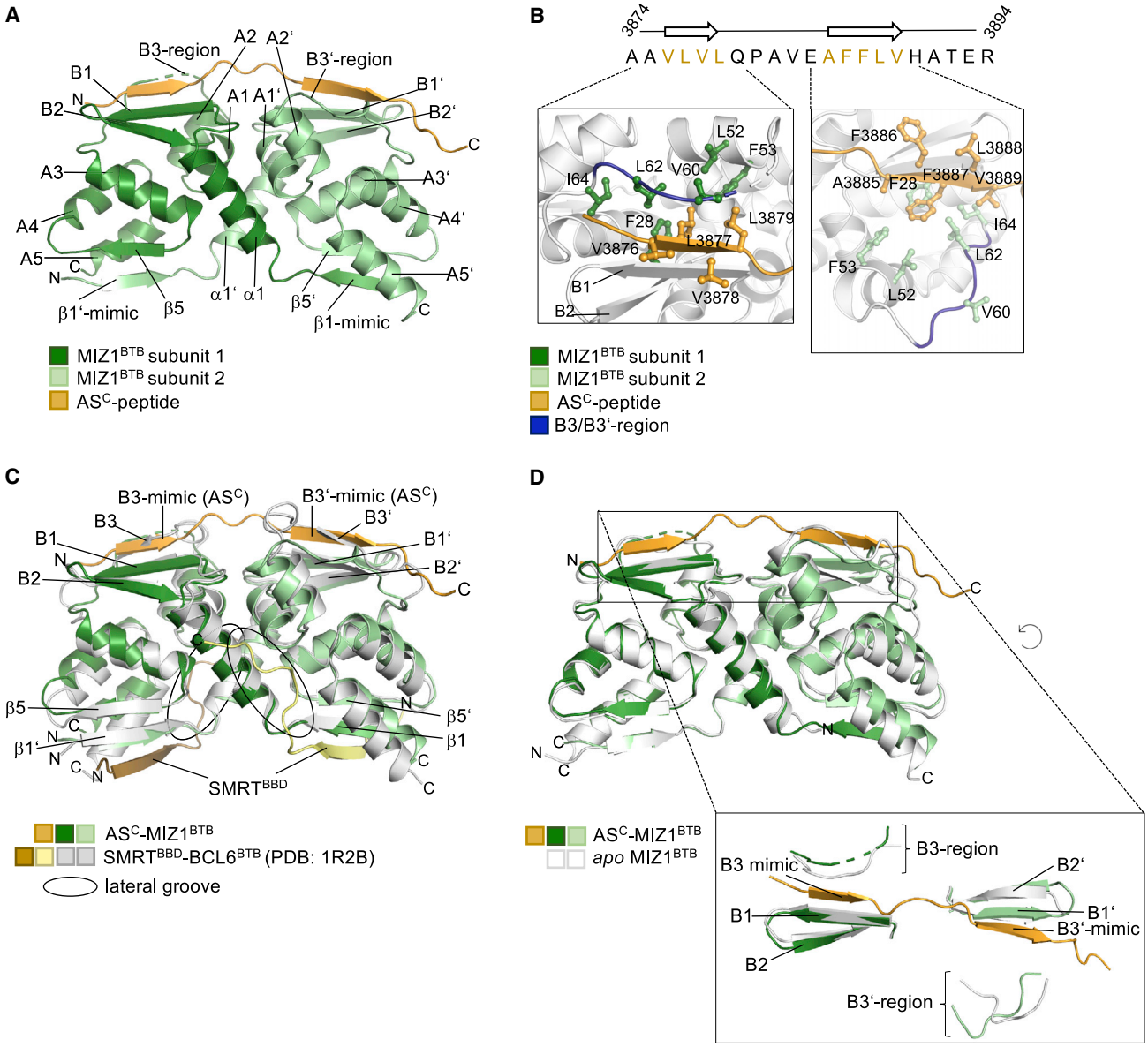

Figure 3. Local conformational flexibility in the BTB domain of MIZ1 enables atypical peptide recognition

(A) Crystal structure of the MIZ1^{BTB} dimer-AS^{C}-peptide complex (this study; PDB: 7AZX). Secondary structural elements of the BTB core are labeled with capital Latin letters and peripheral elements that vary across the BTB domain family with small Greek letters (Stogios et al., 2005); the labels for structural elements of subunit 2 are marked by an inverted apostrophe. A strand of the lower β sheet is denoted "β1-mimic," as it is not part of MIZ1 but a cloning overhang (see Figure S4A).

(B) Detail of the MIZ1^{BTB}-AS^{C} interface in the crystal structure shown in (A). The side chains of residues in the two β strands of AS^{C} and contacting hydrophobic side chains in subunit 1 of the BTB domain dimer are shown in ball-and-stick representation (left panel); the same set of side chains is displayed in subunit 2 (right panel). The amino acid sequence of the AS^{C}-peptide is also shown (top), along with the location of the two β strands formed in the structure (arrows). Those amino acids whose side chains are displayed in the structural panels are highlighted in yellow.

(C) Superposition of the crystal structures of the MIZ1^{BTB}-AS^{C} complex (this study, see A) and BCL6^{BTB} bound to an SMRT-derived peptide (PDB: 1R2B [Ahmad et al., 2003]). BBD denotes BCL6-binding domain. Note that the BCL6-SMRT interaction is of 1:1 stoichiometry; for clarity, the identical peptide ligands were colored differently. The strands of the β sheets that are extended by the peptide ligands are labeled.

(D) Superposition of the crystal structures of MIZ1^{BTB}-AS^{C} (this study, see A) and *apo* MIZ1^{BTB} (this study; PDB: 7AZW). Box: detail of the upper B1-B2 sheet, B3 region, and peptide ligand, extracted from the surrounding protein for clarity. In all panels, visible protein N and C termini are labeled.

such as yet uncharacterized conformational rearrangements of the B3 region, are also conceivable.

To interrogate the atypical MIZ1^{BTB}-AS^{C} interaction functionally, we subjected the entire panel of protein variants to activity assays, monitoring MIZ1 ubiquitination by HUWE1^{AS}. Encouragingly, the mutation-induced effects on MIZ1^{BTB}-AS^{C} binding were mirrored to a large extent in this setup (Figures 4C and 4D): The F28A, V60P, L62A, and I64A substitutions in MIZ1 caused

Please cite this article in press as: Orth et al., Identification of an atypical interaction site in the BTB domain of the MYC-interacting zinc-finger protein 1, Structure (2021), https://doi.org/10.1016/j.str.2021.06.005

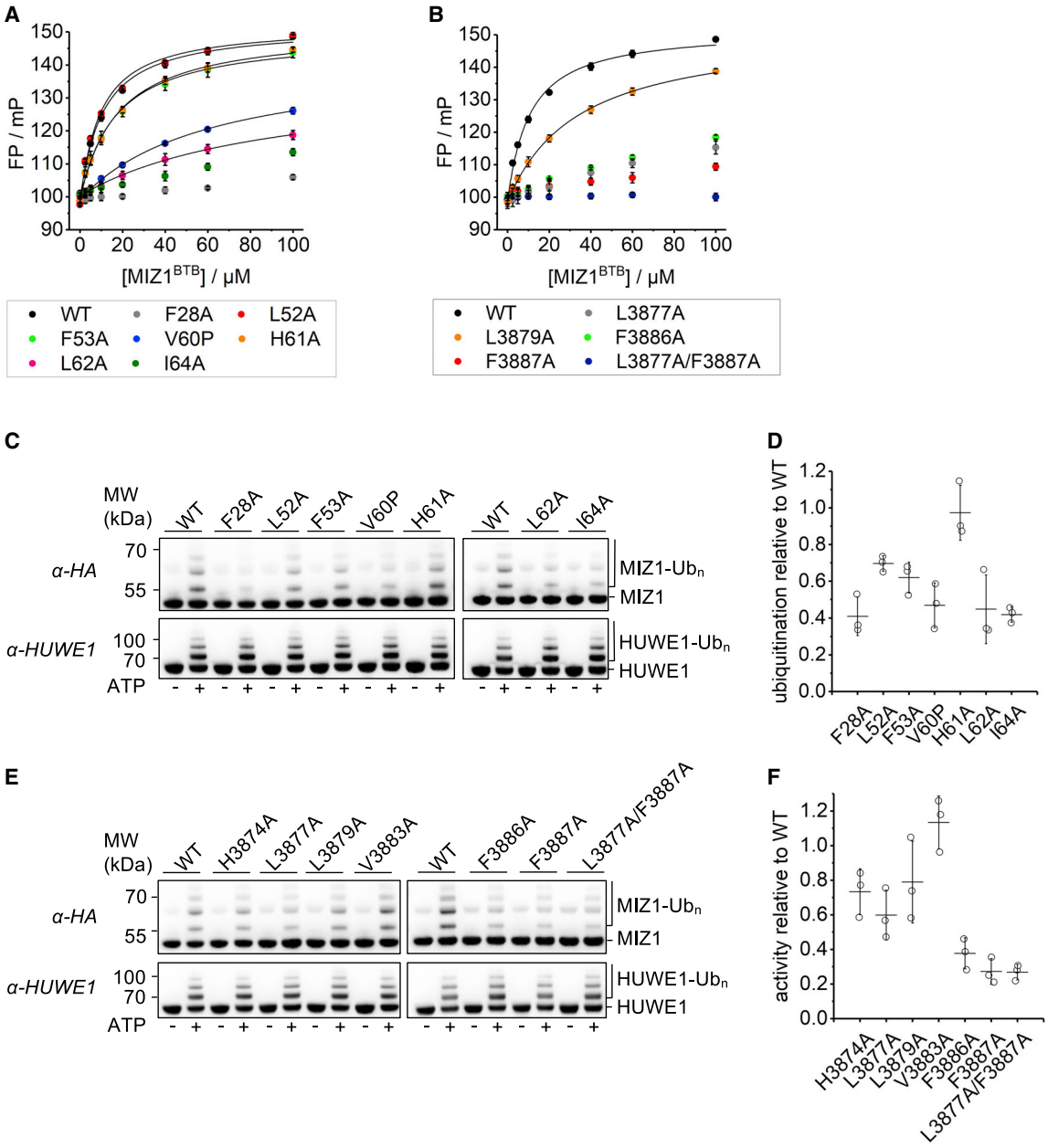

Figure 4. Structure-guided mutagenesis supports the atypical peptide-recognition mode of the BTB domain of MIZ1

(A) FP analysis of the interaction of MIZ1^{BTB} WT and variants thereof, respectively, with a 5-FAM-labeled AS^{C} peptide (HUWE1 residues 3,870–3,894). The mean and SD of three independent experiments were fitted to a single-site binding model, where possible; for the corresponding K_D values, see Table 1.

(B) Analysis analogous to (A), using MIZ1^{BTB} WT and the indicated 5-FAM-labeled AS^{C}-peptide variants.

(C) Representative analysis of the ubiquitination activity of HUWE1^{AS} (residues 3,843–4,374) toward HA-tagged MIZ1$^{1–282}$ WT and variants thereof, respectively. Twenty-minute endpoints were analyzed by SDS-PAGE and anti-HA (MIZ1-ubiquitination and input; top panel) and anti-HUWE1 (E3-autoubiquitination and input; bottom panel) western blotting.

(D) Quantification of ubiquitinated MIZ1 based on three independent assays as shown in (C), normalized to the input amount of MIZ1 (minus ATP lanes). For each variant of MIZ1, the ubiquitination efficiency was plotted relative to the WT (i.e., WT = 1.0). Quantification was done based on three independent replicates using the Image Studio Lite Software (Li-COR; Lincoln, NE, USA; RRID: SCR_013715). The mean and standard deviations were plotted.

(E) Representative analysis of the ubiquitination activities of HUWE1^{AS} WT and variants thereof toward HA-tagged MIZ$^{1-282}$. Details as in (C).

(F) Quantification of ubiquitinated MIZ1 based on three independent assays as shown in (E), normalized to the input amount of HUWE1 (minus ATP lanes). For each mutated variant of HUWE1, the activity was plotted relative to the WT (i.e., WT = 1.0). Quantification was done based on three independent replicates using the Image Studio Lite Software (Li-COR; Lincoln, NE, USA; RRID: SCR_013715). The mean and standard deviations were plotted.

Please cite this article in press as: Orth et al., Identification of an atypical interaction site in the BTB domain of the MYC-interacting zinc-finger protein 1, Structure (2021), https://doi.org/10.1016/j.str.2021.06.005

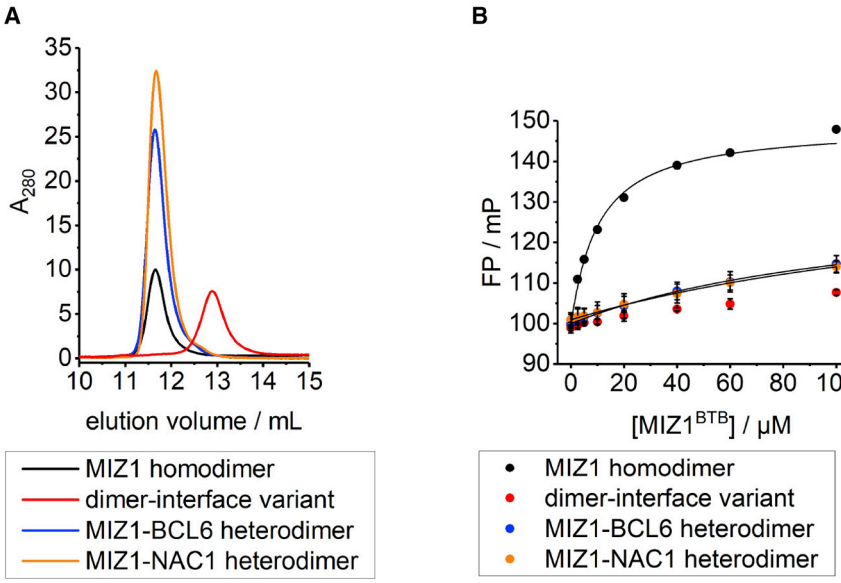

Figure 5. The atypical peptide-binding mode in MIZ1 selects for BTB-domain homodimers over heterodimers and monomers

(A) SEC analyses of the MIZ1^{BTB}-BCL6^{BTB} and MIZ1^{BTB}-NAC1^{BTB} heterodimers, a dimer-interface variant (V10D/L14D/Q17D/V41K) that renders MIZ1^{BTB} monomeric, and MIZ1^{BTB} WT. The peak areas vary due to differences in the respective extinction coefficients.

(B) FP analysis of the interaction of fluorophore-labeled AS^{C} (HUWE1 residues 3,870–3,894) with the same proteins as in (A). The mean and standard deviations of three independent experiments were plotted and fitted to a single-site binding model, where possible; for the corresponding K_D values, see Table 1.

strong reductions in substrate ubiquitination. Slightly weaker effects were observed for the L52A and F53A variants, while the H61A variant was WT-like. Vice versa, marked activity defects were observed for the F3886A, F3887A, and L3877A/F3887A variants of HUWE1^{AS} and weaker effects for H3874A, L3877A, and L3879A; V3883A provided a negative control (Figures 4E and 4F). None of the tested mutations affected the oligomerization state of HUWE1^{AS} (Figure S4D). The mutation-induced activity defects therefore report on the recognition of MIZ1 by the HUWE1^{AS} construct rather than ligase-intrinsic effects.

The atypical binding mode discriminates between homo- and heterodimers of the BTB domain of MIZ1

The bipartite nature of the peptide-binding mode observed in the MIZ1^{BTB} dimer requires a flexible B3 region in both subunits. We thus expected that peptide binding would be reduced in the context of a heterodimeric BTB domain containing one MIZ1 subunit and one subunit from a partner protein with an intrinsic B3 strand. To test this idea, we generated genetically fused heterodimers of MIZ1^{BTB} and BCL6^{BTB} or NAC1^{BTB}, respectively, both of which have a pre-formed B3 strand (Stead and Wright, 2014b) (Figure 5A). FP analyses demonstrated that these heterodimers have only residual AS^{C}-binding capacities, with K_D values of 121 ± 22 μM and 187 ± 20 μM, respectively (Figure 5B and Table 1). In the same vein, we expected that a MIZ1^{BTB} monomer would have a strongly reduced affinity for the AS^{C} peptide compared with a dimer. We introduced mutations into *MIZ1^{BTB}* known to interfere with BTB-domain dimerization (Zhuang et al., 2009) and confirmed the monomeric state of the purified protein variant by SEC (Figure 5A). As we had anticipated, FP analyses yielded no quantifiable affinity of the MIZ1^{BTB} monomer for AS^{C} (Figure 5B and Table 1). Taken together, these studies demonstrate that the recognition of the AS^{C} peptide by MIZ1^{BTB} occurs through an atypical mechanism at the upper B1-B2 sheet. This mechanism requires flexibility in the B3 region of the BTB domain and thereby selects for homodimers over heterodimers or monomers of MIZ1.

DISCUSSION

BTB domains provide multi-functional platforms for the recruitment of diverse protein interactors and allow for integration into a variety of macromolecular complexes. This versatility is thought to be facilitated by the high surface variability of BTB domains, despite their overall conserved architecture, and by varied extensions to their core that generate distinct binding sites. BTB domains in the BTB-ZF, BTB-kelch, and MATH-BTB protein families comprise N-terminal extensions (β1 and/or α1) that drive their dimerization or higher-order self-association (Stogios et al., 2005) and regulate their stability in the cell (Mena et al., 2018, 2020). MATH-BTB-type proteins, such as SPOP, include an additional C-terminal, α-helical extension that serves as a substrate adaptor in cullin-RING-type ubiquitin ligase (CRL) complexes (Zhuang et al., 2009). Analogously, the monomeric BTB domain of SKP1 employs a C-terminal, α-helical extension to recruit substrate-binding F-box proteins to CRLs, but lacks an N-terminal extension (Schulman et al., 2000). Yet another functionally equivalent CRL component to SPOP and SKP1, the single-subunit elongin-C, relies on a minimal BTB core to interact with SOCS-box or VHL-box substrate adaptors (Bullock et al., 2006; Stebbins, 1999). In contrast, the minimal BTB fold of the T1 domain in voltage-gated potassium channels mediates self-association. While these examples illustrate the immense variability of BTB domains across different protein families, it is incompletely understood how functional diversity and specificity are generated in BTB domains of a common protein class.

Our studies reveal that the binding repertoire of BTB-ZF-type transcription factors may be diversified depending on conformational plasticity within the core BTB fold (Figures 6A and 6B). Specifically, we found that the BTB domain of MIZ1 can accommodate a hydrophobic peptide ligand by extending the upper B1-B2 sheet, in lieu of an intrinsic B3 strand. This strand displacement is likely enabled by the flexibility of the B3 region of MIZ1 that exposes a hydrophobic binding groove. In contrast, available structures of BTB domains of other BTB-ZF proteins

Please cite this article in press as: Orth et al., Identification of an atypical interaction site in the BTB domain of the MYC-interacting zinc-finger protein 1, Structure (2021), https://doi.org/10.1016/j.str.2021.06.005

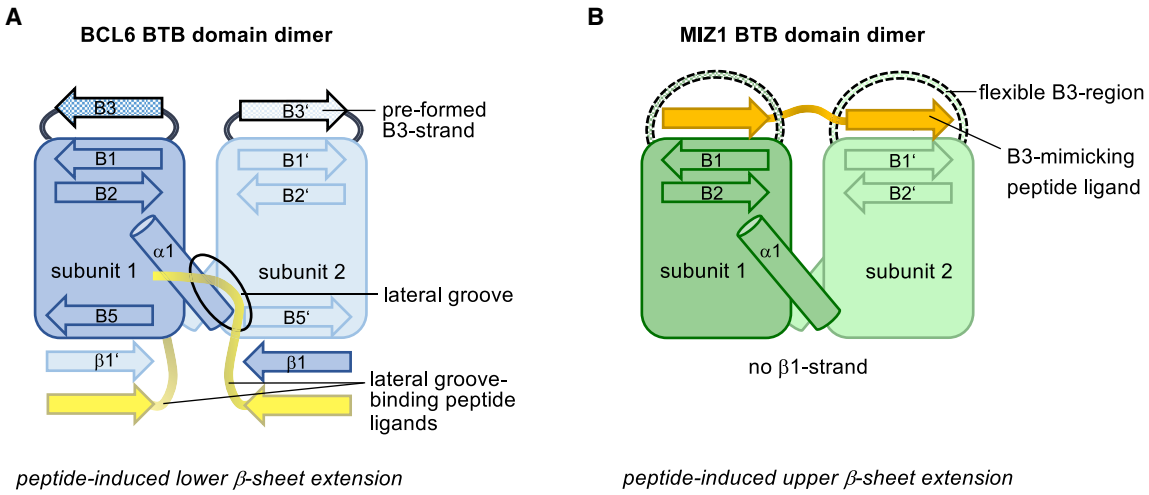

Figure 6. Specific peptide-binding modes in BTB domains

Cartoon representation of two distinct peptide-binding modes observed in BTB domains. (A) Peptide ligands of BCL6 interact with the lateral groove at the dimer interface in each subunit (1:1) and extend a domain-swapped β sheet at the lower end of the BTB-domain monomer (Ahmad et al., 2003; Ghetu et al., 2008). The upper β sheet contains an inherent, intramolecular B3 strand. In contrast, the region that corresponds to the B3 strand of BCL6 is flexible in the BTB domain of MIZ1 (B), thereby allowing for the engagement of peptide ligands that mimic such strands. In the structure we determined, the ligand is a single peptide that spans the BTB dimer interface. This binding mode selects for BTB-domain homodimers over heterodimers with other BTB domains, since both subunits require a flexible B3 region to accommodate the peptide in a bipartite fashion.

contain a pre-formed B3 strand, regardless of their origin, oligomerization state, or engagements with ligands. The sole outlier, to our knowledge, is a crystal structure of the BTB domain of murine PATZ1, which also contains a non-conserved, 23-residue insertion within the B3 region (Piepoli et al., 2020). We thus propose that plasticity in the B3 region may contribute to the functional specialization of certain BTB-ZF proteins and hold specific interaction opportunities.

In contrast to the lateral groove that drives co-repressor interactions in BCL6, the binding site we identified in MIZ1 is sensitive to the dimerization mode and selects for homo- over heterodimers of the BTB domain. Structurally, this sensitivity is rooted in the bipartite nature of the binding site that spans the dimeric subunit interface and involves a ligand-induced β-sheet extension on either side (Figure 6B). Since the majority of BTB domains capable of dimerizing with MIZ1 in the cell may not support the displacement of their pre-formed B3-strand, we predict the identified binding mode selects for MIZ1 homodimers. Another difference between MIZ1- and BCL6-type BTB domains lies in the absence of a β1 strand and the associated lower β sheet in MIZ1 (Figures 6A and 6B). Interestingly, the conformational dynamics of the β1 strand are critical for the stability-based selection of BTB homodimers in the context of CRL-mediated dimerization quality control (Mena et al., 2018, 2020).

Future studies will be required to interrogate which cellular interactors recognize the identified atypical binding site in the BTB domain of MIZ1. A yet unreleased cryo-electron microscopy reconstruction of full-length HUWE1 shows the AS buried, but residues in this region participate in a dynamic intermolecular interface that affects ligase activity (Hunkeler et al., 2020). Although the precise mechanisms and consequences of the conformational dynamics of HUWE1 are still unclear, it is conceivable that regions of HUWE1 other than the AS occupy the binding site we defined in MIZ1. Alternatively, the binding site may function in the recognition of other interactors, which specifically associate with the BTB domain of MIZ1 but lack a BTB domain for heterodimerization. The data presented here may thus provide a basis for sequence-based predictions of candidate MIZ1-binding motifs in the human proteome. The unusual accessibility of the identified binding site in the BTB domain of MIZ1 compared to other BTB domains renders it a prospective target site for peptidomimetic or small-molecule-based manipulations of the macromolecular network of MIZ1 with intriguing therapeutic applications.

STAR★METHODS

Detailed methods are provided in the online version of this paper and include the following:

- KEY RESOURCES TABLE
- RESOURCE AVAILABILITY
  - Lead contact
  - Materials availability
  - Data and code availability
- EXPERIMENTAL MODEL AND SUBJECT DETAILS
- METHOD DETAILS
  - DNA constructs
  - Synthetic peptides
  - Antibodies
  - Recombinant protein preparation
  - Activity assays
  - Analytical size-exclusion chromatography
  - Fluorescence polarization
  - Isothermal titration calorimetry
  - Multi-angle light scattering
  - X-ray crystallography

SUPPLEMENTAL INFORMATION

Supplemental information can be found online at https://doi.org/10.1016/j.str.2021.06.005.

ACKNOWLEDGMENTS

We acknowledge the research training group "Understanding ubiquitylation: from molecular mechanisms to disease" (DFG, GRK2243 to S.L. and M.E.), the Emmy Noether Program of the DFG (LO 2003/1-1,2 to S.L.), and the EMBO Young Investigator Program (to S.L.). B.O. and B.S. were members of the GRK2243. We thank Julia Haubenreisser and the staff of the DESY and ESRF for technical assistance.

AUTHOR CONTRIBUTIONS

Conceptualization, B.O., B.S., and S.L.; Methodology, A.M., K.D., and S.L.; Investigation, B.O. and B.S.; Writing – original draft, B.O., and S.L.; Writing – review & editing, B.O., B.S., A.M., K.D., and S.L.; Funding acquisition, M.E. and S.L.; Supervision, S.L.

DECLARATION OF INTERESTS

S.L. is a member of the advisory board of *Structure*.

Received: December 9, 2020
Revised: March 26, 2021
Accepted: June 4, 2021
Published: June 28, 2021

REFERENCES

Adams, P.D., Afonine, P.V., Bunkóczi, G., Chen, V.B., Davis, I.W., Echols, N., Headd, J.J., Hung, L.-W., Kapral, G.J., Grosse-Kunstleve, R.W., et al. (2010). PHENIX: a comprehensive Python-based system for macromolecular structure solution. Acta Crystallogr. D Biol. Crystallogr. *66*, 213–221.

Adhikary, S., Marinoni, F., Hock, A., Hulleman, E., Popov, N., Beier, R., Bernard, S., Quarto, M., Capra, M., Goettig, S., et al. (2005). The ubiquitin ligase HectH9 regulates transcriptional activation by Myc and is essential for tumor cell proliferation. Cell *123*, 409–421.

Ahmad, K.F., Melnick, A., Lax, S., Bouchard, D., Liu, J., Kiang, C.-L., Mayer, S., Takahashi, S., Licht, J.D., and Privé, G.G. (2003). Mechanism of SMRT corepressor recruitment by the BCL6 BTB domain. Mol. Cell *12*, 1551–1564.

Aravind, L., and Koonin, E.V. (1999). Fold prediction and evolutionary analysis of the POZ domain: structural and evolutionary relationship with the potassium channel tetramerization domain. J. Mol. Biol. *285*, 1353–1361.

Bellenie, B.R., Cheung, K.-M.J., Varela, A., Pierrat, O.A., Collie, G.W., Box, G.M., Bright, M.D., Gowan, S., Hayes, A., Rodrigues, M.J., et al. (2020). Achieving in vivo target depletion through the discovery and optimization of benzimidazolone BCL6 degraders. J. Med. Chem. *63*, 4047–4068.

Berman, H., Henrick, K., and Nakamura, H. (2003). Announcing the worldwide Protein Data Bank. Nat. Struct. Mol. Biol. *10*, 980.

Bullock, A.N., Debreczeni, J.É., Edwards, A.M., Sundström, M., and Knapp, S. (2006). Crystal structure of the SOCS2-elongin C-elongin B complex defines a prototypical SOCS box ubiquitin ligase. Proc. Natl. Acad. Sci. U S A *103*, 7637–7642.

Cardenas, M.G., Yu, W., Beguelin, W., Teater, M.R., Geng, H., Goldstein, R.L., Oswald, E., Hatzi, K., Yang, S.-N., Cohen, J., et al. (2016). Rationally designed BCL6 inhibitors target activated B cell diffuse large B cell lymphoma. J. Clin. Invest. *126*, 3351–3362.

Cerchietti, L.C., Yang, S.N., Shaknovich, R., Hatzi, K., Polo, J.M., Chadburn, A., Dowdy, S.F., and Melnick, A. (2009). A peptomimetic inhibitor of BCL6 with potent antilymphoma effects in vitro and in vivo. Blood *113*, 3397–3405.

Cerchietti, L.C., Ghetu, A.F., Zhu, X., Silva, G.F.D., Zhong, S., Matthews, M., Bunting, K.L., Polo, J.M., Farès, C., Arrowsmith, C.H., et al. (2010). A small-molecule inhibitor of BCL6 kills DLBCL cells in vitro and in vivo. Cancer Cell *17*, 400–411.

Chaharbakhshi, E., and Jemc, J.C. (2016). Broad-complex, tramtrack, and bric-à-brac (BTB) proteins: critical regulators of development. Genesis *54*, 505–518.

Cheng, H., Linhares, B.M., Yu, W., Cardenas, M.G., Ai, Y., Jiang, W., Winkler, A., Cohen, S., Melnick, A., MacKerell, A., et al. (2018). Identification of thiourea-based inhibitors of the B-cell lymphoma 6 BTB domain via NMR-based fragment screening and computer-aided drug design. J. Med. Chem. *61*, 7573–7588.

Cianci, M., Bourenkov, G., Pompidor, G., Karpics, I., Kallio, J., Bento, I., Roessle, M., Cipriani, F., Fiedler, S., and Schneider, T.R. (2017). P13, the EMBL macromolecular crystallography beamline at the low-emittance PETRA III ring for high- and low-energy phasing with variable beam focusing. J. Synchrotron. Radiat. *24*, 323–332.

Emsley, P., and Cowtan, K. (2004). Coot: model-building tools for molecular graphics. Acta Crystallogr. D Biol. Crystallogr. *60*, 2126–2132.

Evans, S.E., Goult, B.T., Fairall, L., Jamieson, A.G., Ferrigno, P.K., Ford, R., Schwabe, J.W.R., and Wagner, S.D. (2014). The ansamycin antibiotic, rifamycin SV, inhibits BCL6 transcriptional repression and forms a complex with the BCL6-BTB/POZ domain. PLoS One *9*, e90889.

Ghetu, A.F., Corcoran, C.M., Cerchietti, L., Bardwell, V.J., Melnick, A., and Privé, G.G. (2008). Structure of a BCOR corepressor peptide in complex with the BCL6 BTB domain dimer. Mol. Cell *29*, 384–391.

Hipps, D.S., Packman, L.C., Allen, M.D., Fuller, C., Sakaguchi, K., Appella, E., and Perham, R.N. (1994). The peripheral subunit-binding domain of the dihydrolipoyl acetyltransferase component of the pyruvate dehydrogenase complex of *Bacillus stearothermophilus*: preparation and characterization of its binding to the dihydrolipoyl dehydrogenase component. Biochem. J. *297*, 137–143.

Hornbeck, P.V., Zhang, B., Murray, B., Kornhauser, J.M., Latham, V., and Skrzypek, E. (2015). PhosphoSitePlus, 2014: mutations, PTMs and recalibrations. Nucleic Acids Res. *43*, D512–D520.

Hunkeler, M., Jin, C.Y., Ma, M.W., Overwijn, D., Monda, J.K., Bennett, E.J., and Fischer, E.S. (2020). Modular HUWE1 architecture serves as hub for degradation of cell-fate decision factors. BioRxiv. https://doi.org/10.1101/2020.08.19.257352.

Braunstein, I.N., Mühlig, H., Musiol, G., and Semendjajew, K.A. (2001). Taschenbuch der Mathematik (Verlag Harri Deutsch).

Jeon, B.-N., Kim, M.-K., Yoon, J.-H., Kim, M.-Y., An, H., Noh, H.-J., Choi, W.-I., Koh, D.-I., and Hur, M.-W. (2014). Two ZNF509 (ZBTB49) isoforms induce cell-cycle arrest by activating transcription of p21/CDKN1A and RB upon exposure to genotoxic stress. Nucleic Acids Res. *42*, 11447–11461.

Kabsch, W. (2010). XDS. Acta Crystallogr. D Biol. Crystallogr. *66*, 125–132.

Kamada, Y., Sakai, N., Sogabe, S., Ida, K., Oki, H., Sakamoto, K., Lane, W., Snell, G., Iida, M., Imaeda, Y., et al. (2017). Discovery of a B-cell lymphoma 6 protein-protein interaction inhibitor by a biophysics-driven fragment-based approach. J. Med. Chem. *60*, 4358–4368.

Katsani, K.R., Hajibagheri, M.A.N., and Verrijzer, C.P. (1999). Co-operative DNA binding by GAGA transcription factor requires the conserved BTB/POZ domain and reorganizes promoter topology. EMBO J. *18*, 698–708.

Keller, S., Vargas, C., Zhao, H., Piszczek, G., Brautigam, C.A., and Schuck, P. (2012). High-precision isothermal titration calorimetry with automated peak-shape analysis. Anal. Chem. *84*, 5066–5073.

Kerres, N., Steurer, S., Schlager, S., Bader, G., Berger, H., Caligiuri, M., Dank, C., Engen, J.R., Ettmayer, P., Fischerauer, B., et al. (2017). Chemically induced degradation of the oncogenic transcription factor BCL6. Cell Rep. *20*, 2860–2875.

Kosan, C., Saba, I., Godmann, M., Herold, S., Herkert, B., Eilers, M., and Möröy, T. (2010). Transcription factor Miz-1 is required to regulate interleukin-7 receptor signaling at early commitment stages of B cell differentiation. Immunity *33*, 917–928.

Lee, K.M., Choi, W.I., Koh, D.I., Kim, Y.J., Jeon, B.N., Yoon, J.H., Lee, C.E., Kim, S.H., Oh, J., and Hur, M.W. (2012). The proto-oncoprotein KR-POK represses transcriptional activation of CDKN1A by MIZ-1 through competitive binding. Oncogene *31*, 1442–1458.

Letunic, I., and Bork, P. (2017). 20 years of the SMART protein domain annotation resource. Nucleic Acids Res. *46*, D493–D496.

McCoull, W., Abrams, R.D., Anderson, E., Blades, K., Barton, P., Box, M., Burgess, J., Byth, K., Cao, Q., Chuaqui, C., et al. (2017). Discovery of pyrazolo[1,5-a]pyrimidine B-cell lymphoma 6 (BCL6) binders and optimization to high affinity macrocyclic inhibitors. J. Med. Chem. *60*, 4386–4402.

McCoull, W., Cheung, T., Anderson, E., Barton, P., Burgess, J., Byth, K., Cao, Q., Castaldi, M.P., Chen, H., Chiarparin, E., et al. (2018). Development of a novel B-cell lymphoma 6 (BCL6) PROTAC to provide insight into small molecule targeting of BCL6. ACS Chem. Biol. *13*, 3131–3141.

McCoy, A.J., Grosse-Kunstleve, R.W., Adams, P.D., Winn, M.D., Storoni, L.C., and Read, R.J. (2007). Phaser crystallographic software. J. Appl. Crystallogr. *40*, 658–674.

Mena, E.L., Kjolby, R.A.S., Saxton, R.A., Werner, A., Lew, B.G., Boyle, J.M., Harland, R., and Rape, M. (2018). Dimerization quality control ensures neuronal development and survival. Science *362*, eaap8236.

Mena, E.L., Jevtić, P., Greber, B.J., Gee, C.L., Lew, B.G., Akopian, D., Nogales, E., Kuriyan, J., and Rape, M. (2020). Structural basis for dimerization quality control. Nature *586*, 452–456.

Möglich, A. (2018). An open-source, cross-platform resource for nonlinear least-squares curve fitting. J. Chem. Educ. *95*, 2273–2278.

Pawson, T., and Nash, P. (2003). Assembly of cell regulatory systems through protein interaction domains. Science *300*, 445–452.

Phan, R.T., Saito, M., Basso, K., Niu, H., and Dalla-Favera, R. (2005). BCL6 interacts with the transcription factor Miz-1 to suppress the cyclin-dependent kinase inhibitor p21 and cell cycle arrest in germinal center B cells. Nat. Immunol. *6*, 1054–1060.

Pickart, C.M., and Raasi, S. (2005). Controlled synthesis of polyubiquitin chains. Methods Enzymol. *399*, 21–36.

Piepoli, S., Alt, A.O., Atilgan, C., Mancini, E.J., and Erman, B. (2020). Structural analysis of the PATZ1 BTB domain homodimer. Acta Crystallogr. D *76*, 581–593.

Piluso, D., Bilan, P., and Capone, J.P. (2002). Host cell factor-1 interacts with and antagonizes transactivation by the cell cycle regulatory factor Miz-1. J. Biol. Chem. *277*, 46799–46808.

Polo, J.M., Dell'Oso, T., Ranuncolo, S.M., Cerchietti, L., Beck, D., Silva, G.F.D., Prive, G.G., Licht, J.D., and Melnick, A. (2004). Specific peptide interference reveals BCL6 transcriptional and oncogenic mechanisms in B-cell lymphoma cells. Nat. Med. *10*, 1329–1335.

Ross, J., Rashkovan, M., Fraszczak, J., Joly-Beauparlant, C., Vadnais, C., Winkler, R., Droit, A., Kosan, C., and Möröy, T. (2019). Deletion of the Miz-1 POZ domain increases efficacy of cytarabine treatment in T- and B-ALL/Lymphoma mouse models. Cancer Res. *79*, 4184–4195.

Sakamoto, K., Sogabe, S., Kamada, Y., Sakai, N., Asano, K., Yoshimatsu, M., Ida, K., Imaeda, Y., and Sakamoto, J. (2017). Discovery of high-affinity BCL6-binding peptide and its structure-activity relationship. Biochem. Biophys. Res. Commun. *482*, 310–316.

Sander, B., Xu, W., Eilers, M., Popov, N., and Lorenz, S. (2017). A conformational switch regulates the ubiquitin ligase HUWE1. eLife *6*, e21036.

Schulman, B.A., Carrano, A.C., Jeffrey, P.D., Bowen, Z., Kinnucan, E.R.E., Finnin, M.S., Elledge, S.J., Harper, J.W., Pagano, M., and Pavletich, N.P. (2000). Insights into SCF ubiquitin ligases from the structure of the Skp1-Skp2 complex. Nature *408*, 381–386.

Silva, G.F.D., Ghetu, A., Cerchietti, L., Polo, J.M., Coop, A., Mackerell, A., Prive, G.G., and Melnick, A. (2007). Design and development of small molecules for specific targeted therapy of diffuse large B-cell lymphoma. Blood *110*, 799.

Stead, M.A., and Wright, S.C. (2014a). Nac1 interacts with the POZ-domain transcription factor, Miz1. Biosci. Rep. *34*, e00110.

Stead, M.A., and Wright, S.C. (2014b). Structures of heterodimeric POZ domains of Miz1/BCL6 and Miz1/NAC1. Acta Crystallogr. Sect F Struct. Biol. Commun *70*, 1591–1596.

Stead, M.A., Trinh, C.H., Garnett, J.A., Carr, S.B., Baron, A.J., Edwards, T.A., and Wright, S.C. (2007). A beta-sheet interaction interface directs the tetramerisation of the Miz-1 POZ domain. J. Mol. Biol. *373*, 820–826.

Stebbins, C.E. (1999). Structure of the VHL-ElonginC-ElonginB complex: implications for VHL tumor suppressor function. Science *284*, 455–461.

Stogios, P.J., Downs, G.S., Jauhal, J.J., Nandra, S.K., and Privé, G.G. (2005). Sequence and structural analysis of BTB domain proteins. Genome Biol. *6*, R82.

Stogios, P.J., Cuesta-Seijo, J.A., Chen, L., Pomroy, N.C., and Privé, G.G. (2010). Insights into strand exchange in BTB domain dimers from the crystal structures of FAZF and Miz1. J. Mol. Biol. *400*, 983–997.

Słabicki, M., Yoon, H., Koeppel, J., Nitsch, L., Burman, S.S.R., Genua, C.D., Donovan, K.A., Sperling, A.S., Hunkeler, M., Tsai, J.M., et al. (2020). Small-molecule-induced polymerization triggers degradation of BCL6. Nature *588*, 164–168.

van der Ent, F., and Löwe, J. (2006). RF cloning: a restriction-free method for inserting target genes into plasmids. J. Biochem. Biophys. Methods *67*, 67–74.

Vonrhein, C., Tickle, I.J., Flensburg, C., Keller, P., Paciorek, W., Sharff, A., and Bricogne, G. (2018). Advances in automated data analysis and processing within autoPROC , combined with improved characterisation, mitigation and visualisation of the anisotropy of diffraction limits using STARANISO. Acta Crystallogr. Sect Found Adv. *74*, a360.

Weber, A., Marquardt, J., Elzi, D., Forster, N., Starke, S., Glaum, A., Yamada, D., Defossez, P., Delrow, J., Eisenman, R.N., et al. (2008). Zbtb4 represses transcription of P21CIP1 and controls the cellular response to p53 activation. EMBO J. *27*, 1563–1574.

Wickliffe, K.E., Lorenz, S., Wemmer, D.E., Kuriyan, J., and Rape, M. (2011). The mechanism of linkage-specific ubiquitin chain elongation by a single-subunit E2. Cell *144*, 769–781.

Wiese, K.E., Walz, S., Eyss, B., von Wolf, E., Athineos, D., Sansom, O., and Eilers, M. (2013). The role of MIZ-1 in MYC-dependent tumorigenesis. CSH Perspect. Med. *3*, a014290.

Winger, J.A., Derbyshire, E.R., Lamers, M.H., Marletta, M.A., and Kuriyan, J. (2008). The crystal structure of the catalytic domain of a eukaryotic guanylate cyclase. BMC Struct. Biol. *8*, 42.

Winn, M.D., Ballard, C.C., Cowtan, K.D., Dodson, E.J., Emsley, P., Evans, P.R., Keegan, R.M., Krissinel, E.B., Leslie, A.G.W., McCoy, A., et al. (2011). Overview of the CCP4 suite and current developments. Acta Crystallogr. D Biol. Crystallogr. *67*, 235–242.

Wolf, E., Gebhardt, A., Kawauchi, D., Walz, S., von Eyss, B., Wagner, N., Renninger, C., Krohne, G., Asan, E., Roussel, M.F., et al. (2013). Miz1 is required to maintain autophagic flux. Nat. Commun. *4*, 2535.

Yasui, T., Yamamoto, T., Sakai, N., Asano, K., Takai, T., Yoshitomi, Y., Davis, M., Takagi, T., Sakamoto, K., Sogabe, S., et al. (2017). Discovery of a novel B-cell lymphoma 6 (BCL6)-corepressor interaction inhibitor by utilizing structure-based drug design. Bioorgan Med. Chem. *25*, 4876–4886.

Ye, B., Lista, F., Coco, F.L., Knowles, D., Offit, K., Chaganti, R., and Dalla-Favera, R. (1993). Alterations of a zinc finger-encoding gene, BCL-6, in diffuse large-cell lymphoma. Science *262*, 747–750.

Zhuang, M., Calabrese, M.F., Liu, J., Waddell, M.B., Nourse, A., Hammel, M., Miller, D.J., Walden, H., Duda, D.M., Seyedin, S.N., et al. (2009). Structures of SPOP-substrate complexes: insights into molecular architectures of BTB-Cul3 ubiquitin ligases. Mol. Cell *36*, 39–50.

Please cite this article in press as: Orth et al., Identification of an atypical interaction site in the BTB domain of the MYC-interacting zinc-finger protein 1, Structure (2021), https://doi.org/10.1016/j.str.2021.06.005

STAR★METHODS

KEY RESOURCES TABLE

REAGENT or RESOURCE	SOURCE	IDENTIFIER
Antibodies		
mouse monoclonal anti-HA-Peroxidase	Sigma-Aldrich	Cat. #: H6533; RRID: AB_439705
rabbit polyclonal anti-HUWE1	Sigma-Aldrich	Cat. #: SAB2900746
Bacterial and virus strains		
E. coli TOP10	Thermo Fisher Scientific	Cat. #: C404006
E. coli LOBSTR-BL21(DE3)-RIL	Kerafast	Cat. #: EC1002
E. coli BL21(DE3)	Thermo Fisher Scientific	Cat. #: C600003
Chemicals, peptides, and recombinant proteins		
HUWE1-peptide for crystallization (residues 3870-3897)	Elim Biopharm	custom
5-FAM-AS^{N} (HUWE1 residues 3843-3869)	Elim Biopharm	custom
AS^{C}-Lys-5-FAM (HUWE1 residues 3870-3894)	Elim Biopharm	custom
ubiquitin	Wickliffe et al., 2011	N/A
UBA1	Wickliffe et al., 2011	N/A
UBCH7	Sander et al., 2017	N/A
HUWE1^{HECT} (residues 3993-4374)	Sander et al., 2017	N/A
HUWE1^{Dmin} (residues 3951-4374)	Sander et al., 2017	N/A
HUWE1^{D} (residues 3896-4374)	Sander et al., 2017	N/A
HUWE1^{AS} (residues 3843-4374)	Sander et al., 2017	N/A
AS (residues 3843-3890, N-terminal lipoyl domain tag)	this paper	N/A
AS^{N} (residues 3843-3869, N-terminal lipoyl domain tag)	this paper	N/A
AS^{C} (residues 3870-3890, N-terminal lipoyl domain tag)	this paper	N/A
MIZ1^{BTB} (residues 1-115)	Stogios et al., 2010	N/A
MIZ1^{BTB} (residues 1-115, with cloning overhang)	Stogios et al., 2010	N/A
MIZ1 (residues 1-282)	this paper	N/A
MIZ1-BCL6 heterodimer	Stead and Wright., 2014b	N/A
MIZ1-NAC1 heterodimer	Stead and Wright., 2014b	N/A
Deposited data		
crystal structure of MIZ1^{BTB}	this paper	PDB: 7AZW
crystal structure of a MIZ1^{BTB}-AS^{C} complex	this paper	PDB: 7AZX
crystal structure of MIZ1^{BTB}	Stead et al., 2007	PDB: 2Q81
crystal structure of MIZ1^{BTB}	Stogios et al., 2010	PDB: 3M52
crystal structure of BCL6^{BTB} in complex with a SMRT-derived peptide	Ahmad et al., 2003	PDB: 1R2B
Experimental models: organisms/strains		
Sf9 insect cells	Expression Systems	RRID: CVCL_0549

(*Continued on next page*)

Please cite this article in press as: Orth et al., Identification of an atypical interaction site in the BTB domain of the MYC-interacting zinc-finger protein 1, Structure (2021), https://doi.org/10.1016/j.str.2021.06.005

Continued

REAGENT or RESOURCE	SOURCE	IDENTIFIER
Oligonucleotides		
codon-optimized BCL6^{BTB} with linker to generate MIZ1-BCL6 heterodimer: TGCCCTCAAGTCACTTGCTCGTAGTGGTG GCGGGTCGAGC GGGGGTTCCGGTACCG CAGATTCTTGCATCCAATTTACACGTCATG CGTCTGACGTTCTGTTGAACCTTAATCGCT TACGCTCTCGCGACATTCTTACAGACGTT GTGATCGTCGTCTCTCGCGAGCAGTTTCG CGCACATAAGACTGTTTTGATGGCCTGCT CA GGATTATTCTACTCTATTTTCACTGATC AATTGAAATGCAACCTGTCGGTGATTAATC TTGATCCGGAGATCAATCCTGAG GGGTT CTGCATCTTACTTGATTTCATGTACACATC TCGTTTG AACCTTCGTGAGGGTAATATCA TGGCGGTCATGGCTACC GCCATGTATTTA CAAATGGAGCACGTCGTGGACACCTGCC GTAAGTTTATTAAAGCCTCCGAATGATAAT ACCACCTCATCGAATGC	Stead and Wright., 2014b; IDT	N/A
codon-optimized NAC1^{BTB} with linker to generate MIZ1-NAC1 heterodimer: TGCCCTCAAGTCACTTGCTCGCTCCGGTG GCGGGTCGAGCGGAGGAAGCGGGACAG CACAGACTTTGCAGATGGAGATT CCTAAC TTTGGAAATTCTATCCTTGAATGCCTGAAT GAGCAACGCTTACAGGGGTTATACTGTGA CGTTTCGGTTGTTGTG AAGGGTCATGCCT TCAAGGCTCATCGCGCCGTATTGGCGGCC TCGAGTTCGTACTTCCGCGATCTTTTTAATA ATTCTCGTAGTGCTGTAGTGGAACTGCCAG CGGCAGTACAACCTCAGTCTTTTCAGCAGA TTCTGTCATTCTGTTATACAGGTCGCTTAAG CATGAACGTCGGGGATCAAGATTTACTGA TGTACACTGCC GGTTTCTTGCAGATCCAAG AAATCATGGAGAAAGGTACG GAATTCTTCC TGAAGGTAAGTAGTTGATAATACCACCTCA TCGAATGC	Stead and Wright., 2014b; IDT	N/A
Recombinant DNA		
ubiquitin	Wickliffe et al., 2011	N/A
UBA1	Wickliffe et al., 2011	N/A
UBCH7	Sander et al., 2017	N/A
HUWE1^{HECT} (residues 3993-4374)	Sander et al., 2017	N/A
HUWE1^{Dmin} (residues 3951-4374)	Sander et al., 2017	N/A
HUWE1^{D} (residues 3896-4374)	Sander et al., 2017	N/A
HUWE1^{AS} (residues 3843-4374)	Sander et al., 2017	N/A
AS (residues 3843-3890, N-terminal lipoyl domain tag)	this paper	N/A
AS^{N} (residues 3843-3869, N-terminal lipoyl domain tag)	this paper	N/A
AS^{C} (residues 3870-3890, N-terminal lipoyl domain tag)	this paper	N/A
MIZ1^{BTB} (residues 1-115)	Stogios et al., 2010	N/A
MIZ1^{BTB} (residues 1-115, with cloning overhang)	Stogios et al., 2010	N/A
MIZ1 (residues 1-282)	this paper	N/A
MIZ1-BCL6 heterodimer	Stead and Wright., 2014b	N/A
MIZ1-NAC1 heterodimer	Stead and Wright., 2014b	N/A

(*Continued on next page*)

Please cite this article in press as: Orth et al., Identification of an atypical interaction site in the BTB domain of the MYC-interacting zinc-finger protein 1, Structure (2021), https://doi.org/10.1016/j.str.2021.06.005

Continued

REAGENT or RESOURCE	SOURCE	IDENTIFIER
Software and algorithms		
XDS	Kabsch, 2010	http://xds.mpimf-heidelberg.mpg.de/
XSCALE	Kabsch, 2010	http://xds.mpimf-heidelberg.mpg.de/
STARANISO	Vonrhein et al., 2018	http://staraniso.globalphasing.org/cgi-bin/staraniso.cgi
CCP4	Winn et al., 2011	http://www.ccp4.ac.uk/
Phenix	Adams et al., 2010	http://www.phenix-online.org/
Coot	Emsley and Cowtan., 2004	https://www2.mrc-lmb.cam.ac.uk/personal/pemsley/coot/
Pymol 1.7.6	Schrödinger, LLC	https://www.schrodinger.com/suites/pymol/
ImageStudio Lite Software	LI-COR Biosciences	https://www.licor.com/bio/image-studio/
ASTRA6	Wyatt Technology	https://www.wyatt.com/products/software/astra.html
NITPIC	Keller et al., 2012	http://biophysics.swmed.edu/MBR/software.htm
OriginPro 9.4	OriginLab Corporation	http://microcal-origin.software.informer.com/

RESOURCE AVAILABILITY

Lead contact

Further information and requests for resources and reagents should be directed to and will be fulfilled by the lead contact, Sonja Lorenz (sonja.lorenz@mpibpc.mpg.de).

Materials availability

All unique/stable reagents generated in this study are available from the lead contact without restriction.

Data and code availability

The crystal structures generated in this study were deposited in the Protein Data Bank (PDB) with the accession codes PDB: 7AZW ($MIZ1^{BTB}$) and PDB: 7AZX ($MIZ1^{BTB}$-AS^{C}-complex).

EXPERIMENTAL MODEL AND SUBJECT DETAILS

All proteins used for biochemical, biophysical, and structural studies were recombinantly expressed in *E. coli* LOBSTR-BL21(DE3)-RIL (Kerafast, Boston, MA, USA), *E. coli* BL21(DE3) (Thermo Fischer Scientific, Waltham, MA, USA), or *S. frugiperda* (*Sf9*) cells (RRID: CVCL_0549). For cloning, *E. coli* TOP10 cells (Thermo Fisher Scientific) were used. All genes are of human origin. For further information, see method details.

METHOD DETAILS

DNA constructs

Cloning and mutagenesis were performed by ligation-free methods (van der Ent and Löwe, 2006). The human gene constructs for $HUWE1^{HECT}$ (residues 3993-4374), $HUWE1^{Dmin}$ (residues 3951-4374), $HUWE1^{D}$ (residues 3896-4374), $HUWE1^{AS}$ (residues 3843-4374) were previously described (Sander et al., 2017). In short, the genes were inserted into a modified pBADM11 vector (EMBL Heidelberg), coding for an N-terminal TEV protease-cleavable His_6-tag. The expression vector for UBCH7 was also described previously (Sander et al., 2017) and contains the *UBCH7* gene, kindly provided by M. Rape (Berkeley, CA, USA), in a modified pSKB2-backbone (derived from pET28a (Merck, Darmstadt, Germany)), encoding an N-terminal *Rhinovirus* 3C protease-cleavable His_6-SUMO-tag. The UBA1 construct in pFASTBac (Thermo Fisher Scientific, Waltham, MA, USA), kindly provided by Michael Rape, and the ubiquitin gene, inserted into pet30A (Novagen, Madison, WI, USA) at the Nde1 and HindIII restriction sites, were also described previously (Sander et al., 2017; Wickliffe et al., 2011). The HUWE1 constructs AS (residues 3843-3890), AS^{N} (residues 3843-3869), and AS^{C} (residues 3870-3890) were cloned into a modified pSKB2-vector (derived from pET28a (Merck, Darmstadt, Germany)) (Winger et al., 2008) encoding an N-terminal lipoyl domain-tag (residues 2–85 of branched-chain alpha-keto acid dehydrogenase subunit E2 from *Geobacillus stearothermophilus* (Hipps et al., 1994)) and a C-terminal His_6-tag. The coding sequence for $MIZ1^{BTB}$ (residues 1-115) was cloned into a a pET23 (for X-ray crystallography) and a modified pSKB2 vector (for interaction studies), both encoding an N-terminal, TEV protease-cleavable His_6-lipoyl domain-tag (resulting in an N-terminal GGSMAS-overhang based on the pET23

Please cite this article in press as: Orth et al., Identification of an atypical interaction site in the BTB domain of the MYC-interacting zinc-finger protein 1, Structure (2021), https://doi.org/10.1016/j.str.2021.06.005

and GGSMA-overhang based on the pSKB2 vector, respectively, after TEV protease-cleavage). Additionally, the coding sequences for MIZ1^{BTB} (residues 1-115), the MIZ1^{BTB}-BCL6^{BTB,} and the MIZ1^{BTB}-NAC1^{BTB} fusion proteins (genes synthesized by Integrated DNA Technologies (Coralville, IA, USA); the domain boundaries were chosen based on previous protocols (Stead and Wright, 2014b)) were cloned into a pCCA-1-vector encoding an N-terminal, ULP1-cleavable His$_6$-SUMO-tag (Wickliffe et al., 2011). The MIZ1 construct comprising residues 1-282 (MIZ1$^{1-282}$) was expressed from a pETM41-vector encoding an N-terminal, TEV protease-cleavable MBP-tag and a C-terminal HA-His$_6$-tag.

Synthetic peptides

The HUWE1-derived peptides comprising residues 3870-3897 (for X-ray crystallography), N-terminally 5-FAM (5-carboxyfluorescein)-labeled AS^N (residues 3843-3869), and AS^C-Lys-5-FAM (residues 3870-3894; with the label attached to the ε-amino group of the added C-terminal lysine) were synthesized by Elim Biopharm (Hayward, CA, USA) at > 95 % purity.

Antibodies

For Western blotting, anti-HA-peroxidase-coupled mouse monoclonal (H6533; Sigma-Aldrich; St. Louis, MO, USA; RRID: AB_439705) and anti-HUWE1 rabbit polyclonal (SAB2900746; Sigma-Aldrich) antibodies were used.

Recombinant protein preparation

UBA1, UBCH7, and ubiquitin were purified as previously described (Sander et al., 2017; Wickliffe et al., 2011). In brief, UBA1 was expressed in *Sf9* cells and purified by Nickel (Ni)-affinity chromatography, followed by a gel filtration (Superdex 200 column, GE Healthcare, Chicago, IL, USA) in 50 mM Tris, 150 mM NaCl, 5% glycerol, 2 mM DTT, pH 7.5. UBCH7 was expressed in BL21(DE3) cells and purified by Ni-affinity chromatography, 3C protease-cleavage of the affinity tag, and a final gel filtration (Superdex 75 column, GE Healthcare) in 25 mM Tris, 100 mM NaCl, 2 mM DTT, pH 7.5). Ubiquitin was expressed in BL21(DE3) cells and purified by perchlorid acid precipitation, cation exchange chromatography (HiTrap Sp-HP column, GE Healthcare), and a final gel filtration (Superdex 75 column, GE Healthcare), based on established protocols (Pickart and Raasi, 2005). All other proteins were expressed in LOBSTR RIL cells at 15 °C for 16 to 18 hours after induction with 0.05 % L-arabinose or 0.5 mM IPTG. In brief, HUWE1^{HECT}, HUWE1^{Dmin}, HUWE1^{D}, HUWE1^{AS} were purified as previously described (Sander et al., 2017). For HUWE1^{HECT}, HUWE1^{Dmin}, HUWE1^{D}, HUWE1^{AS}, cells were lysed in 80 mM HEPES pH 8, 500 mM NaCl, 10 % glycerol, 20 mM imidazole and 5 mM β-mercaptoethanol, in the presence of protease inhibitor cocktail (Roche, Basel, Switzerland), followed by Ni-affinity chromatography and over-night dialysis (in 20 mM HEPES (pH 8.0), 250 mM NaCl, 10 mM imidazole and 3 mM β-mercaptoethanol) at 4 °C in the presence of TEV-protease. After removal of the protease and uncleaved protein by Ni-affinity chromatography, a gel filtration was performed (HiLoad 16/600 Superdex 75 column (GE Healthcare) for HUWE1^{HECT} and HiLoad 16/600 Superdex 200 column (GE Healthcare) for HUWE1^{Dmin}, HUWE1^{D}, and HUWE1^{AS}, respectively) in 20 mM HEPES pH 8, 150 mM NaCl, 1 mM EDTA and 5 mM DTT. All other HUWE1 and MIZ1 constructs used here were purified according to the same protocols (Sander et al., 2017), but with two modifications: (i) the respective affinity tags were not cleaved off the AS, AS^N, AS^C constructs; (ii) for the preparation of MIZ1$^{1-282}$, the imidazole concentration was lowered to 5 mM in the lysis and dialysis buffers. For the AS, AS^N, AS^C, MIZ1^{BTB}, MIZ1^{BTB}-BCL6^{BTB}, and MIZ1^{BTB}-NAC1^{BTB} proteins, the final gel filtration steps were performed with a HiLoad 16/600 Superdex 75 column (GE Healthcare). For MIZ1$^{1-282}$, a HiLoad 16/600 Superdex 200 column (GE Healthcare) was used.

Activity assays

0.2 μM UBA1, 5 μM UBCH7, 5 μM HUWE1^{AS} (WT or mutated variant), 100 μM ubiquitin, 12 μM MIZ1$^{1-282}$ (WT or mutated variant) were incubated with 3 mM ATP and 8 mM $MgCl_2$ in 25 mM HEPES, pH 7.4 at 37 °C for 20 minutes. MIZ1$^{1-282}$ was used because the BTB domain of MIZ1 is not ubiquitinated in the cell (Hornbeck et al., 2015). The reactions were quenched by the addition of reducing loading dye and analyzed by SDS-PAGE and Western blotting. The input and reaction products were quantified with the Image Studio Lite Software (Li-COR; Lincoln, NE, USA; RRID: SCR_013715). The mean and standard deviations from three independent experiments were plotted. Additional details are provided in the corresponding figure legends.

Analytical size-exclusion chromatography

For interaction studies, the proteins (150 μM of AS^N, AS^C, AS, HUWE1^{D}, HUWE1^{AS}, respectively, and 300 μM of MIZ1^{BTB}) were injected onto a Superdex 200 Increase 3.2/300 column (GE Healthcare) in 20 mM HEPES, pH 8.0, 100 mM NaCl, 1 mM EDTA, and 5 mM DTT at 4 °C The eluted protein fractions were analyzed by SDS-PAGE and Coomassie staining. To compare the oligomerization states of MIZ1^{BTB} WT, mutated variants thereof, and the fusion constructs, respectively, the proteins were injected onto a Superdex 75 10/300 GL Increase column (GE Healthcare) at a concentration of 100 μM. In the case of HUWE1^{D}, HUWE1^{AS} WT, and mutated variants thereof, a protein concentration of 50 μM and a Superdex 200 10/300 GL Increase column (GE Healthcare) was used.

Fluorescence polarization

FP measurements were performed in black, non-binding, flat-bottom, 384-well microplates (Greiner Bio-One, Frickenhausen, Germany) at 30 °C, using a Clariostar microplate reader (BMG-Labtech, Ortenberg, Germany) with excitation and emission wavelengths of 540 and 590 nm, respectively. All proteins and 5-FAM-labeled peptides were in 20 mM HEPES, pH 8.0, 150 mM NaCl, 1 mM EDTA, 5 mM DTT, and 0.01 % Triton X-100 with a constant peptide concentration of 1 μM. To derive a dissociation constant, K_D, for the

MIZ1^{BTB}-AS^{C} interaction, averaged binding curves from three independent experiments were fitted to a single-site binding model with OriginPro 9.4 (OriginLab Corporation; Northhampton, MA, USA; RRID: SCR_002815):

$$FP = FP_f + \left(\left(\frac{FP_b - FP_f}{2L}\right)\right) \cdot \left((L + c + K_D) - \sqrt{(L + c + K_D)^2 - 4 \cdot L \cdot c}\right)$$

where FP = fluorescence polarization, FP_b = fluorescence polarization for the bound state, FP_f = fluorescence polarization for the unbound state, and L = concentration of fluorophore-labeled peptide.

To analyze the interaction of the HUWE1^{Dmin} protein with the AS^{N}-ligand, the averaged binding curves from three independent experiments were fitted to a competition model that accounts for both protein-ligand binding and protein dimerization:

$$P + L \rightleftarrows PL, \text{ dissociation constant } K_{D1}$$

$$P + P \rightleftarrows P2, \text{ dissociation constant } K_{D2}$$

where P = unbound protein monomer, P2 = unbound protein dimer, L = unbound ligand, and PL = protein-ligand complex.

This reaction scheme gives rise to a third-order polynomial for P (unbound protein):

$$P^3 + P^2 \cdot \left(1 + 2 \cdot \frac{K_{D1}}{K_{D2}}\right) \cdot \frac{K_{D2}}{2} + P \cdot (K_{D1} + L_0 - P_0) \cdot \frac{K_{D2}}{2} - K_{D1}P_0 \cdot \frac{K_{D2}}{2} = 0$$

The only real third root of the polynomial was calculated using Cardano's formula (Braunstein et al., 2001). With the knowledge of P, the values of P2, L, and PL can be determined. The fluorescence polarization signal was then fitted with Fit-o-mat (Möglich, 2018) to

$$FP = L/L_0 \times FP_f + PL/L_0 \times FP_b$$

where L_0 is the total concentration of the fluorophore-labeled peptide.

Isothermal titration calorimetry

ITC was performed with a Microcal ITC$_{200}$ calorimeter (GE Healthcare) at 37°C. The proteins were dialyzed into 20 mM HEPES, pH 8.0, 100 mM NaCl, 1 mM EDTA, and 1 mM ß-mercaptoethanol over night. 60 μM MIZ1^{BTB} was applied to the sample cell and 810 μM AS^{C} (with an N-terminal lipoyl domain-tag) to the syringe of the calorimeter. The reference cell was filled with buffer. Titration experiments included 15 injections of 2.7 μl in 240-second intervals. The reference cell power was set to 6 μcal/sec and the stirring speed to 300 rpm. The data were fitted to a single-site binding model with the NITPIC (Keller et al., 2012), yielding the changes in the free energy (ΔG), enthalpy (ΔH), entropy (ΔS), as well as the dissociation constant (K_D) and the stoichiometry (n).

Multi-angle light scattering

300 μM of AS^{C} (with N-terminal lipoyl domain-tag) and 500 μM of MIZ1^{BTB}, respectively, were injected onto a Superdex 200 10/300 GL column (GE Healthcare) in 20 mM HEPES, pH 8.0, 150 mM NaCl, 1 mM EDTA, and 5 mM DTT at RT. The column was coupled to a Dawn 8+ MALS detector and an Optilab T-rEX refractive index detector (Wyatt Technology; Santa Barbara, CA, USA). Molecular weights were determined at the absorbance peak tips with ASTRA 6 (Wyatt Technology; RRID: SCR_016255).

X-ray crystallography

MIZ1^{BTB} *apo* crystals grew at 4.9 mg/mL and 20°C in hanging drops containing 0.1 mM sodium acetate and 8 % PEG4000, pH 4.6. The same conditions including 26.7 % glycerol were used for cryo-protection. Diffraction data were collected at beamline P13 of the PETRA III storage ring at DESY (Hamburg, Germany) (Cianci et al., 2017). Data processing was performed with XDS (RRID: SCR_015652) (Kabsch, 2010) and molecular replacement with Phaser (McCoy et al., 2007), as implemented in CCP4 (RRID: SCR_007255) (Winn et al., 2011), using PDB 3M52 (Stogios et al., 2010) as a search model.

Crystals of the MIZ1^{BTB}-AS^{C}-peptide complex grew in hanging drops and two similar conditions: (i) 3 mg/mL MIZ1^{BTB} with a 1.2-fold excess of AS^{C} in 125 mM sodium acetate and 6 % PEG4000, pH 4.6. (ii) 5 mg/mL MIZ1^{BTB} with a 1.2-fold excess of AS^{C} in or 100 mM sodium acetate and 4 % PEG4000, pH 4.6. For cryo-protection, 30 % glycerol and 1.3 mM AS^{C} (corresponding to a 2.5-fold molar excess over the MIZ1^{BTB} concentration) were included in the respective mother liquor. Diffraction data were collected at beamline ID30A-3 of the ESRF (Grenoble, France). Two data sets obtained from crystals grown in either condition were processed with XDS, merged with XSCALE (RRID: SCR_015652) (Kabsch, 2010), and analyzed with STARANISO (RRID: SCR_018362) (Vonrhein et al., 2018). Molecular replacement was performed with Phaser, as implemented in Phenix (RRID: SCR_014224) (Adams et al., 2010), using PDB 3M52 (Stogios et al., 2010) as a search model. The use of STARANISO resulted in weak reflections being excluded, and thus a reduced number of reflections was used during the refinement (see Table 2). Both structures were refined with phenix.refine (RRID: SCR_016736) (Adams et al., 2010) using individual B-factors; model building was performed in Coot (RRID: SCR_014222) (Emsley and Cowtan, 2004) and model validation with the PDB validation server (Berman et al., 2003) . All structural representations were created with PyMOL (RRID: SCR_000305) (open source, V1.7.6; DeLano Scientific LLC).